Cement and Concrete Research 84 (2016) 8–19

Contents lists available at ScienceDirect

Cement and Concrete Research

journal homepage: www.elsevier.com/locate/cemconres

Viscosity prediction of cement-filler suspensions using interference model: A route for binder efficiency enhancement

Bruno L. Damineli [a], Vanderley M. John [a], Björn Lagerblad [b], Rafael G. Pileggi [a,*]

[a] Department of Construction Engineering, Escola Politécnica, University of São Paulo, 05508-900 São Paulo, Brazil
[b] Department of Construction Engineering, Royal Institute of Technology, SE-100 44 Stockholm, Sweden

ARTICLE INFO

Article history:
Received 22 May 2015
Accepted 17 February 2016
Available online xxxx

Keywords:
Cement paste (D)
Filler (D)
Rheology (A)
Particle size distribution (B)
Modelling

ABSTRACT

Producing cementitious materials with low CO_2 emissions is a key challenge for sustainability, considering the increasing demand for cement and the inefficacy of current industrial solutions. Improving the efficiency of binder use is mandatory, so that binder replacement by inert fillers with lower environmental loads is an alternative, which demands careful control of the rheological behaviour to decrease the water demand of pastes. Dispersion and packing models are well known, but other less explored parameters of raw materials (surface area, density, roughness) and paste (water content, distance between particles) determine the interaction among particles, affecting the paste's rheological behaviour.

The aim of this paper is to assess the influence of inert fillers on the rheological behaviour of cementitious pastes. A range of 12 inert fillers with varied aspects was evaluated. The results indicated a good agreement between the Casson viscosity and the interference parameter calculated using the interference model.

1. Introduction

Due to the demands in housing and infrastructure of the developing countries, cement production and related CO_2 emissions are increasing steadily; as a result, the industry is under pressure to reduce CO_2 emissions due to global warming constraints [1,2]. The current strategies used for decreasing CO_2 emissions – kiln efficiency, use of renewable fuels, and clinker replacement by blast-furnace slag and fly ash – have limits and will not prevent emissions to grow [2–4]. Carbon capture and storage could double the cement cost [5–7], which would primarily affect the poorest and neediest countries.

New options based on the improvement of binder use efficiency must be developed [8]. The partial replacement of clinker and reactive supplementary cementitious materials (SCMs) by progressively higher fractions of low-cost, widely available low CO_2 footprint mineral fillers is a better option than any calcined materials. The challenge is to develop low-binder products with performances and durability similar to those of the conventional high binder ones [9]. Limestone filler production releases from 26 to 75g CO_2/kg of material [10–11] mostly during the milling process, reducing CO_2 emissions proportionally to the increase of limestone content [12] and several other mineral fillers can be added to limestone as low footprint SCMs.

Since most of these mineral fine particles do not react with water [13,14], the amount of inert filler must be controlled in order to control porosity ensuring competitive mechanical performance and durability. In practical terms, the amount of water needed to achieve appropriate rheological behavior defines the maximum filler content. This might be one reason the actual average filler content in cement is around 6% despite the 34% limit in the European standard [15].

Efficient clinker–inert filler systems must have lower water content (vol./vol.) than the conventional systems with the adequate rheological behavior during mixing, transportation, and casting. This can be achieved by techniques of packing and dispersion of particles [16], even if packing models do not predict water demand since their unique aim is to calculate the volume of empty space among the particles. They usually assume particles as perfect spheres, ignoring surface area, morphology, and particles interactions. Most packing models also ignore the way the particles interfere on each other's movement during flow in highly concentrated suspensions. Divergences between predicted values of porosity and experimental results are assumed to be related to wall effects and irregularities in particles shapes, so they are considered in more advanced models [17].

In this scenario, models aiming to predict the amount of water to provide suitable rheological behavior are of practical interest. More precisely, both yield stress and viscosity parameters need prediction.

Regarding yield stress, significant progress in predictive models is observed in literature, as reported by Buscall et al., Kapur et al., Scales et al., Zhou et al., and Flatt & Bowen [18–22]. These researchers modeled different aspects of the suspensions, including particles size

* Corresponding author.
E-mail addresses: bruno.damineli@usp.br (B.L. Damineli), vmjohn@lme.pcc.usp.br (V.M. John), bjorn.lagerblad@cbi.se (B. Lagerblad), rafael.pileggi@usp.br (R.G. Pileggi).

http://dx.doi.org/10.1016/j.cemconres.2016.02.012
0008-8846/

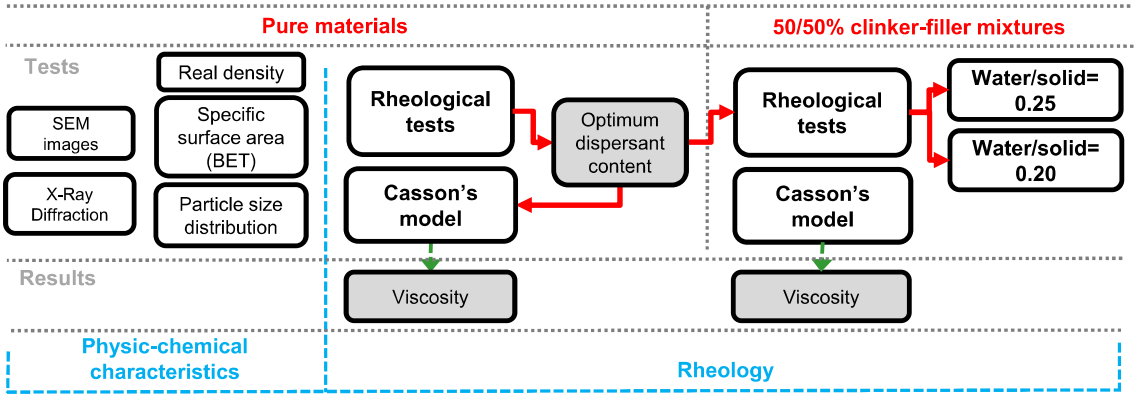

Fig. 1. Experimental planning flowchart.

distributions, volume fraction of solids, inter-particle forces, radius of curvature at particles contacts, etc.

Similar approach for viscosity forecast still need investigation, since most traditional models are based on packing factors [23–27]. A proposal to overcome this lack is the *Particles Interference Model* [28], which succeeded in correlating several physical aspects of particles and the immersing fluid in order to predict the viscosity of alumina ceramic suspension. This model has not been tested in Portland cement mixtures.

For this reason, the present paper aims to explore the Particles Interference Model to predict the viscosity of highly concentrated water suspensions of Portland cement with fillers with different mineralogical composition, when dispersed with admixtures.

2. Experimental setup

A CEM I 42.5 cement and a dozen of different fillers of four distinct mineralogical characteristics and particles smaller than 63 μm were tested, as well as 50/50 wt% cement-filler combined systems. The flowchart in Fig. 1 summarises the experimental plan, highlighting the materials characterization testing methods and the rheological evaluation program.

2.1. Materials

The fillers were named according to their predominant mineralogical characteristics: "D" = dolomite, "C" = calcite, "Q" = quartz, and "G" = granite. "Cem1" is the cement CEM I–42.5. All tested materials were commercially available in the Swedish market.

2.1.1. Chemical and mineralogical and characterization

Table 1 presents the chemical characterization results of the raw materials based on a semi-quantitative X-ray fluorescence analysis performed using a PANalytical Axios Advanced instrument. Table 2 presents mineralogical compositions of the raw materials evaluated by X-ray diffraction analysis using a PANalytical X'Pert PRO instrument equipped with an X'Celerator detector, as quantified by Rietveld method using PANalytical Inorganic Structure Database.

2.1.2. Physical characterisation

The powders were evaluated using the following testing methods:

1) particle-size distribution was determined using a Malvern Mastersizer laser diffraction granulometer, on liquid environment using water, pre-treatment on ultrasound dispersion for 2 min;
2) specific surface area was determined using the BET method with Gemini 2375 equipment, Micromeritics;
3) true density of particles was determined using a He picnometer Quantachrome MVP 5DC;
4) scanning electron microscopy (SEM) images were obtained using a Quanta 600FEG instrument.

The testing conditions for SEM images were as follows: 1) vacuum mode—high vacuum; 2) HV—10.00 kV; 3) det—ETD; 4) spot—2.0. The parameters of Mag and WD were varied.

Fig. 2 shows the particle size distributions of the tested materials. Table 3 presents values of the specific surface area (BET), the particles true density, and the calculated shape factor (ShF), herein defined as the ratio between the BET surface area and the theoretical surface area [29] calculated from the laser particle size distribution (Fig. 2), assuming that all of the particles are perfect spheres [30]. A high value of ShF indicates that particles deviate substantially from a spherical shape as a consequence of their shape and roughness. A ShF value close to 1 corresponds to a spherical, smooth particle. The calculated deviation from a spherical shape was confirmed by SEM micrographic analysis, as shown in Fig. 3.

The results shown in Table 3 and Fig. 3 make evident the need for extending the evaluation of particles beyond only size distribution. As a consequence, it is necessary to consider other characteristics to understand the rheological behaviour of cement-filler suspensions.

Table 1
Chemical compositions of the raw materials obtained via X-ray fluorescence (X-Ray PANalytical Axios Advanced).

Oxides (%)	Cem1	D1	D2	D3	C1	C2	C3	Q1	Q2	G1	G2	G3	G4
CaO	65.4	30.0	29.3	28.3	53.8	54.7	55.2	–	–	1.09	6.45	0.98	3.65
SiO_2	18.9	4.59	4.45	8.76	2.62	1.69	0.44	98.9	98.1	72.6	54.8	70.5	63.3
Al_2O_3	3.09	0.39	0.80	0.85	0.41	0.05	0.05	–	–	13.8	14.4	14.5	15.5
Fe_2O_3	5.27	0.58	0.53	0.66	0.15	0.11	0.05	–	–	1.97	10.70	2.33	6.53
MgO	0.68	21.40	21.30	21.20	0.19	0.15	0.87	–	–	0.32	3.44	0.55	1.83
SO_3	4.19	–	–	–	–	–	–	–	–	–	–	–	–
K_2O	0.78	0.05	0.21	0.28	0.05	0.05	0.05	–	–	5.22	2.56	5.68	3.78
Na_2O	0.09	0.05	0.05	0.05	0.05	0.05	0.05	–	–	3.24	2.63	2.81	2.84
TiO_2	0.22	0.05	0.05	0.05	0.05	0.05	0.05	–	–	0.25	1.76	0.22	0.84
Other	0.43	0.19	0.21	0.05	0.18	0.35	0.34	0.95	1.48	0.97	1.69	0.92	0.72

Table 2
Mineralogical compositions of the raw materials determined by X-ray diffraction (PANalytical X'Pert PRO equipped with an X'Celerator detector) using the semi-quantitative Rietveld method (PANalytical Inorganic Structure Database).

		Material												
Compound	Chemical formula	Cem1	D1	D2	D3	C1	C2	C3	Q1	Q2	G1	G2	G3	G4
Alite	Ca_3SiO_5	*****												
Brownmillerite	Ca_2FeAlO_5	**												
Calcium sulfate hemyhydrate	$CaSO_4\ 0.5H_2O$	**												
Calcite	$CaCO_3$	*	*	*	*	******	******	******						
Dolomite	$CaMg(CO_3)_2$		******	******	******			*						
Quartz	SiO_2		*		*	*	*		******	******	****	***	****	****
Cristobalite	SiO_2													
Tridymite	SiO_2													
Chalk	$Mg_3(Si_2O_5)_2(OH)_2$		*	*										
Albite	$(Na,Ca)Al(Si,Al)_3)_8$										***	***	***	***
Clinochlore	$(Mg_{2,96}Fe_{1,55}Fe_{0,136}Al_{1,275})$ $(Si_{2,622}Al_{1,376}O_{10})(OH)_8$		*	*	*						*	**	*	*
Microcline	$K(AlSi_3)O_8$										****	***	***	***
Muscovite	$(K_{0,82}Na_{0,18})(Fe_{0,03}Al_{1,97})\ (AlSi_3)O_{10}(OH)_2$										*		**	**
Phlogopite	$KMg_3Si_3AlO_{10}(F,OH)_2$			*	*							**		
Amphibole	$Al_{3,2}Ca_{3,4}Fe_{4,02}K_{0,6}Mg_6\ NaSi_{12,8}O_{44}(OH)_4$		*	*	*							**		**
Nefeline	$KNa_3(AlSiO_4)_4$													
Ortoclase	$KAlSi_3O_8$													

Note: 6 stars ≥ 85%; 5 stars = 50–85%; 4 stars = 30–50%; 3 stars = 16–30%; 2 stars = 6–15%; 1 star = 1–5%.

2.2. Rheological characterization

2.2.1. Mixing procedure and rheological test

The mixing procedure was defined for 2 kg of powder and a predefined volume of water placed into the mixing bowl. Water content criteria for pure cement and combined cement-filler systems are described in the subsequent sections. The suspensions were mixed for 5 min using the following sequence: 1) add water in the bowl, 2) start the mixer at low-speed, 3) add powder slowly to the water during low-speed mixing up to 2 min, 4) increase the speed to high (at this time, all of the powder has been added), 5) mix at this condition for 3 min.

After mixing, the rheological tests were performed via a Physica MCR 300 rheometer using a single-gap cylinder CC27 (outer radius = 14.46 mm, gap = 1.13 mm, sample volume = 19.35 ml, max shear rate = 300 s^{-1}, max shear stress = 2800 Pa, cylinder with vertical grooves). Paste samples (~19.35 ml) were placed into the rheometer cup for shear stress evaluation under continuously increasing shear rates from 0 to 200 s^{-1} (1 min—acceleration), followed by a decrease in shear rate from 200 to 0 s^{-1} in six steps (200, 150, 100, 50, 25, and 10 s^{-1}) of 30 s each. The recorded shear stress for each shear rate was the penultimate measurement in each step, when the suspension was stabilised in the corresponding shear rate.

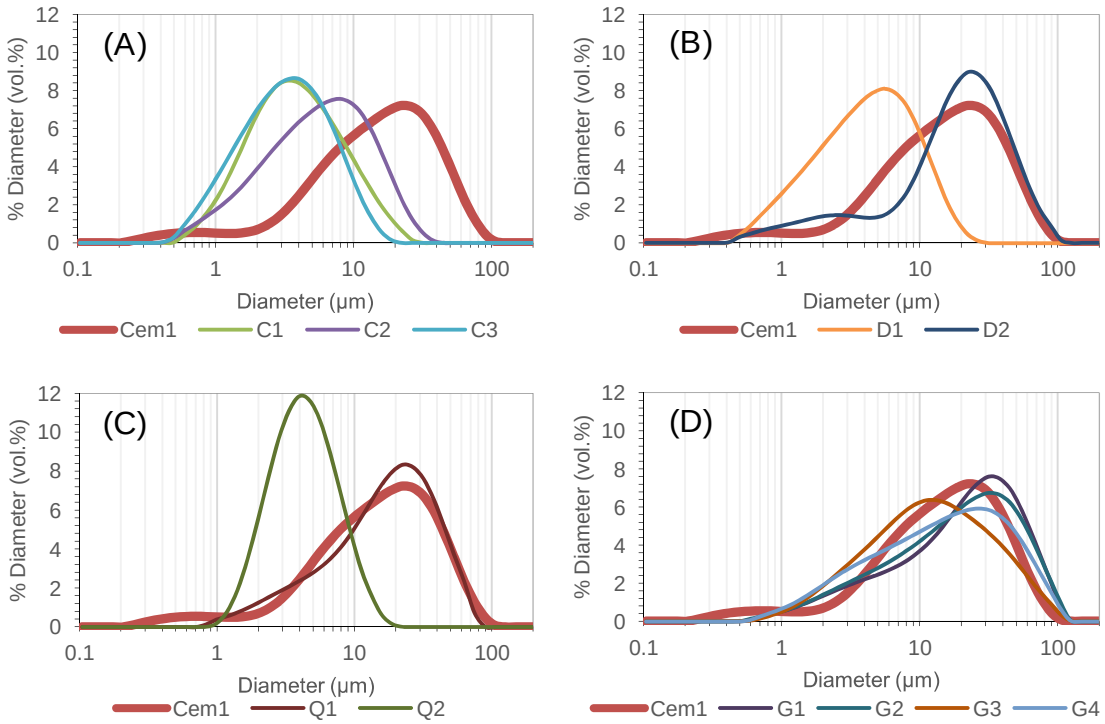

Fig. 2. Particle size distribution of the tested fillers compared to cement CEM 1 (Malvern Mastersizer laser diffraction granulometer): (A) cement and calcite, (B) cement and dolomite, (C) cement and quartz, (D) cement and granite.

Table 3
Particle true density (He picnometer) (Quantachrome MVP 5DC), specific surface area (BET) (Gemini 2375, Micromeritics), and calculated shape factor (ShF) of the studied materials.

Material	Particle true density (g/cm^3)	Specific surface area (m^2/g)	Shape factor ($m^2/g/m^2/g$)
Cem 1	3.20	0.816	2.60
D1	2.82	4.420	5.91
D2	2.82	1.202	4.07
C1	2.70	3.956	5.06
C2	2.70	1.361	2.16
C3	2.70	3.195	3.43
Q1	2.65	0.996	3.96
Q2	2.65	4.052	6.52
G1	2.67	1.665	6.66
G2	2.67	2.290	8.44
G3	2.67	3.810	11.54
G4	2.67	2.824	8.77

Fig. 4 describes the steps of the mixing procedure and rheological test.

The first rheological tests were performed on pure materials to determine the optimum dispersant content – a commercial polycarboxylate-based material (Glenium 51, BASF) – that allows for reaching the lowest suspension viscosity. In sequence, cement-filler systems were prepared and tested with the ideal amount of dispersant.

2.2.2. Pure materials

The lowest water/solid ratio (w/s) to mix each tested system was defined by gradually adding water inside the fixed mass of powder material (2 kg) up to the point where the suspension could be mixed [31] with no dispersants at a low-speed shear rate in a Hobart mixer. Therefore, the chosen w/s provided the highest practicable solid concentration, thus ensuring adequacy for rheological tests. This procedure also aims to reproduce practical situations where water content is defined based on workability.

Subsequently, the optimum dispersant content for each pure material was defined by increasing the amounts of admixture (at this point, w/s was fixed according previous definition) and assessing the viscosity diminution up to stability, which indicates the optimum dispersant content (minimum content to reach minimum viscosity), expressed as weight percentage (wt.%) of the mass of solid. The apparent viscosity calculated (shear stress and shear rate ratio) at the maximum shear rate of 200 s^{-1} was adopted as the viscosity criteria. Fig. 5 displays an example of the "dispersant content *versus* apparent viscosity" graphic for granite G1.

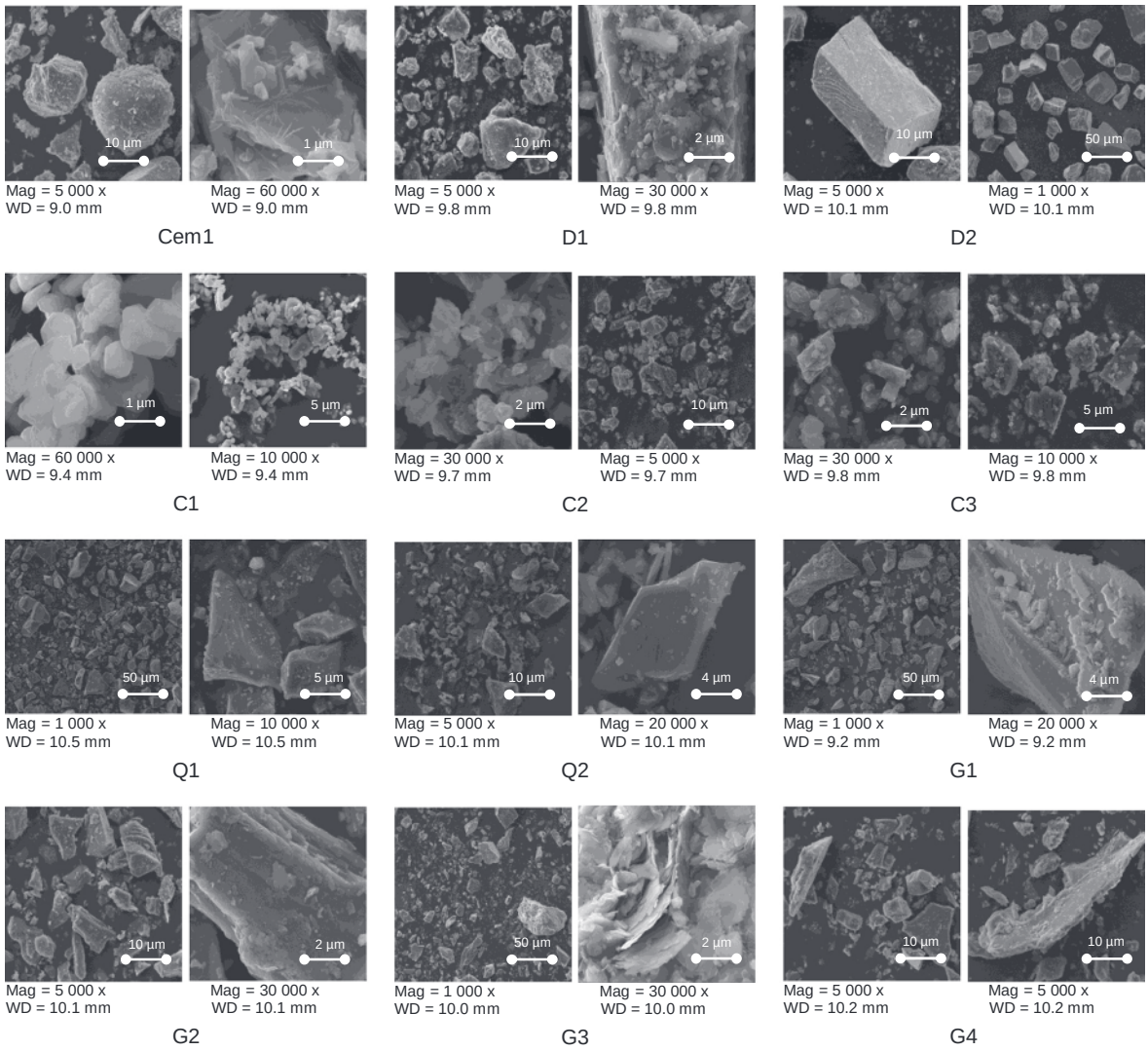

Fig. 3. Scanning electron microscopy images of cement CEM 1 and the tested fillers using a Quanta 600FEG instrument. Fixed parameters for all micrographs: 1) vacuum mode—high vacuum; 2) HV—10.00 kV; 3) det—ETD; 4) spot—2.0. The parameters of magnification (Mag) and working distance (WD) are indicated under each image.

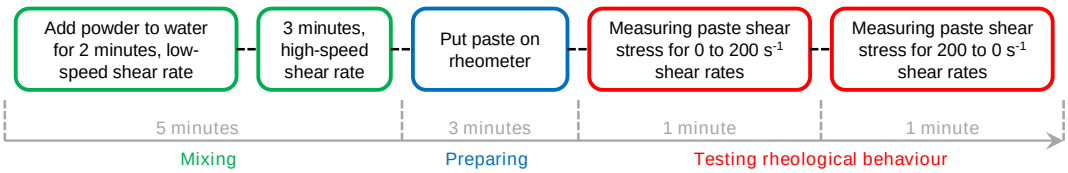

Fig. 4. Flowchart of the procedure of mixing suspensions and the rheological testing methodology.

For this case, at a dispersant content above 0.25wt.%, the rheological behaviour measured is considered representative of the system where particles are individualised moving units flowing inside the liquid, thus reflecting the particle size distribution measured via laser diffraction (Fig. 2). The optimum dispersant content (wt.%) and the calculated specific dispersant content per unit of surface area (mg/m^2) are presented in Table 4 for all of the tested systems, as well as the water/solid ratio defined for the suspensions. The rheological parameters are also presented in Table 4.

2.2.3. Blended cement-filler pastes

The 50/50% cement-filler paste viscosities were measured using the same rheological evaluation continuous flow test procedure described in Section 2.2.3. The suspensions were prepared with an estimated dispersant content to ensure the full dispersion of all particles. The calculated dispersant amount was the weight average value between the optimum polycarboxylate content for the pure individual raw materials, thus adjusting the dispersant content for the true particle surface area present in the suspension. This approach is based on the good dispersion efficiency of the chosen dispersant for all of the fillers and cement at alkaline pH [32–34] and the lack of expected cement-filler reactive interaction in very short times [35–36]. All blended systems were tested with w/s = 0.25, and the compositions with lowest viscosities were also evaluated with lower water contents. Table 4 summarises the water content in each blended tested system, the calculated dispersant amount (wt.%) and the amount of dispersant per unit of surface area. This table also presents the rheological parameters for the tested suspensions.

3. Results and discussion

3.1. Water/solid ratio, optimum dispersant content, and rheological parameters

Table 4 exhibits the water/solid ratio defined for the suspensions and the measured optimum dispersant content (wt.%). The calculated specific dispersant content per unit of surface area (mg/m^2) is also presented for all of the tested systems, as well as the measured apparent viscosity at the maximum shear rate of 200 s^{-1} and the yield stress.

Bearing in mind the main objective of the present work, the rheological results were further evaluated through Casson's model [37] to determine Casson's viscosity, thus determining the suspension viscosity not dependent on the shear rate. Table 4 presents confident values of Casson's viscosity for all the tested system (correlation coefficient $R^2 \sim 0.9$).

The experimental setup adopted to prepare the suspensions clearly resulted in a great dispersion of viscosities as visualised in Table 4. Despite being possible to produce low-viscosity cement-fillers suspensions, this experimental approach enhances the difficulty of using fillers because no predictability was evident. In fact, the systematic use of fillers requires predictive models capable of correlating the individual particle characteristics to the measured rheological parameters.

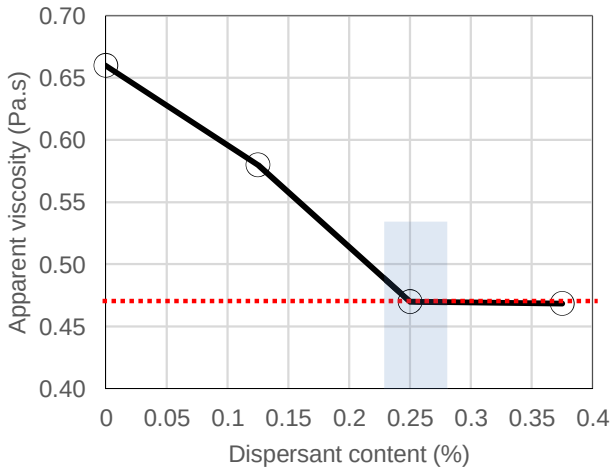

Fig. 5. Example of the optimum dispersant content determination for G1. The shaded area highlights the minimum dispersant amount (0.25wt.%) for dispersion stability in this suspension.

3.2. Viscosity prediction models

Traditional viscosity prediction models (see Table 5), such as the models of Krieger–Dougherty, Mooney, and Quemada [23–27], aim to predict relative viscosity by correlating the volumetric solid content to a certain critical solid content supported by the suspension. However, experimentally adjusted parameters are necessary before being able to forecast the suspension's viscosities.

Table 4
Water/solid ratio, optimum dispersant content (wt.%), specific dispersant content (mg/m^2), apparent viscosity (η_{ap}), yield stress (τ_o), Casson viscosity (η_c) of the tested systems.

System		w/s	Optimum disp. (wt%)	Specific disp. (mg/m^2)	η_{ap} (Nm.s)	τ_o (MPa)	η_c (Nm.s)
Pure	Cem1	0.25	0.375	4.60	0.68	4.12	0.6084
	Cem1	0.275	0.375	4.60	0.49	1.93	0.4189
	D1	0.40	1.00	2.26	0.24	0.73	0.2133
	D2	0.30	0.375	3.12	0.42	1.01	0.3699
	C1	0.45	1.125	2.84	0.14	4.76	0.09109
	C2	0.30	0.25	1.84	0.28	1.96	0.259
	C3	0.35	0.75	2.35	0.26	2.19	0.2373
	Q1	0.40	0.50	5.02	0.42	0.64	0.4224
	Q2	0.425	0.75	1.85	0.11	0.24	0.0782
	G1	0.40	0.25	1.50	0.47	2.67	0.4438
	G2	0.40	0.375	1.64	0.75	5.01	0.7055
	G3	0.375	0.50	1.31	0.86	3.48	0.8178
	G4	0.40	0.375	1.33	1.03	5.94	0.981
Blended	Cem1 + D1	0.25	0.688	2.63	1.02	3.11	0.8478
	Cem1 + D1	0.20	0.688	2.63	3.18	15.50	2.679
	Cem1 + D2	0.25	0.375	3.72	0.67	1.67	0.5746
	Cem1 + C1	0.25	0.75	3.14	0.91	5.44	0.8169
	Cem1 + C2	0.25	0.313	2.88	0.53	2.37	0.4735
	Cem1 + C2	0.20	0.313	2.88	1.39	4.18	1.204
	Cem1 + C3	0.25	0.563	2.81	0.64	3.17	0.5541
	Cem1 + C3	0.20	0.563	2.81	1.61	5.43	1.32
	Cem1 + Q1	0.25	0.438	4.83	0.89	1.40	0.7062
	Cem1 + Q2	0.25	0.563	2.31	0.76	5.05	0.6453
	Cem1 + G1	0.25	0.313	2.52	1.04	2.29	0.9569
	Cem1 + G2	0.25	0.375	2.41	1.28	2.18	1.078
	Cem1 + G3	0.25	0.438	1.89	1.42	6.07	1.259
	Cem1 + G4	0.25	0.375	2.06	1.35	2.03	1.104

Table 5
Equations of the viscosity predictive models of Krieger–Dougherty [23], Mooney [24], Eilers [25], Quemada [26], and Robinson [27]. Table extracted from [38].

Reference	Equation
Krieger and Dougherty [27]	$\eta_r = (1 - \phi/\varphi_T)^{-[\eta]\varphi_T}$
Mooney [28]	$\eta_r = \exp(-[\eta]\phi/(1-\phi/\varphi_T))$
Eilers [29]	$\eta_r = 1 + [\eta]\phi/2(1-\phi/\varphi_T)^{2}$
Quemada [30]	$\eta_r = (1 - \phi/\varphi_T)^{-2}$
Robinson [31]	$\eta_r = 1 + [\eta]\phi(1-\phi/\varphi_T)$

η_r = relative viscosity; $[\eta]$ = intrinsic viscosity; ϕ = solid content; φ_T = critical solid content.

Despite the search for understanding what governs critical solid content [38], these experimental models are not yet based on the fundamental properties of particles and liquids that compose the suspensions because the experimental parameters must be defined for each set of combined materials, thus preventing them from being considered true predictive models.

An attempt to develop a predictive model to explain the great range of obtained viscosities is based on calculating the mean interparticle separation distance (IPS) of the suspensions using the equation proposed by Funk and Dinger [39–40]:

$$IPS = \frac{2}{VSA} x \left[\frac{1}{V_s} - \frac{1}{1 - P_{of}} \right] \quad (1)$$

where VSA = volumetric surface area (m^2/cm^3), calculated by the product of specific surface area SSA (m^2/g) and solid density ρ_s (g/cm^3); Vs = volumetric solid fraction on suspension; and P_{of} = pore fraction in the maximum packing condition calculated using the Westman and Hugill model [39,41].

According to these authors, the viscosity diminishes by increasing IPS, due to the larger space for particle motion in well-dispersed suspensions. This condition reduces shearing energy dissipation due to particle interactions.

The characteristics of the pure materials are presented in Figs. 2 and 3 and Table 3. Information about the pure and blended suspensions is presented in Table 4. Fig. 6 displays the blended particle size distributions, and Table 6 presents the measured and calculated characteristics for all of the granular systems considered according to the volumetric proportion of the materials in the blended systems, including the calculated IPS values of the tested suspensions. It is unmistakable that fillers exert an influence on the surface area, particle density, and particle packing porosity, thereby affecting the IPS.

Fig. 7 presents only the correlation of IPS and Casson's viscosity, but a similar trend would also be perceived for apparent viscosity, given the proximity between the measured and the calculated viscosities, as shown in Table 4. In fact, it is possible to establish a linear relationship between both viscosities with a coefficient of 0.86 and a standard deviation greater than 0.99. In view of the comprehensive significance of Casson's model, their values will be adopted for outlining the following discussions.

As seen in Fig. 7, there is a poor correlation in viscosity due to the increase in IPS. In fact, below 0.4 μm, the IPS displayed no relationship regarding the viscosity. The observed lack of a trend is reasonable because assuming the mean distance among all of the particles (IPS) as a sort of degree of freedom regarding mobility neglects the well-established knowledge that demonstrated the existence of steric interference on a suspension's particle mobility when the ratios of the diameters among the particles are less than 10 [39,42], even in well-dispersed systems. In fact, only particles with a diameter less than one-tenth that of the larger particles do not interfere with the movement of the coarser ones; in these cases, the fines are considered as part of the fluid.

As stated by Farris [42], the viscosity of a multimodal suspension can be modelled as a combination of the unimodal viscosities defined by each particle within the system, if the relative sizes are adequate to prevent interaction between large and fine particles, hence ensuring that each size is completely independent of the other.

Despite the veracity of this statement, two critical aspects must be highlighted. The first aspect is the need of experimental parameters to describe viscosity of suspensions in which the particle diameter ratio is below 10 [39,42], in order to measure interparticle interference in suspension mobility. The second aspect is that even to predict the viscosity of the unimodal suspensions through traditional rheological models, there is a requirement for experimental measurements to define the equations parameters. Consequently, it is possible to infer that the current knowledge for viscosity description of multimodal suspensions

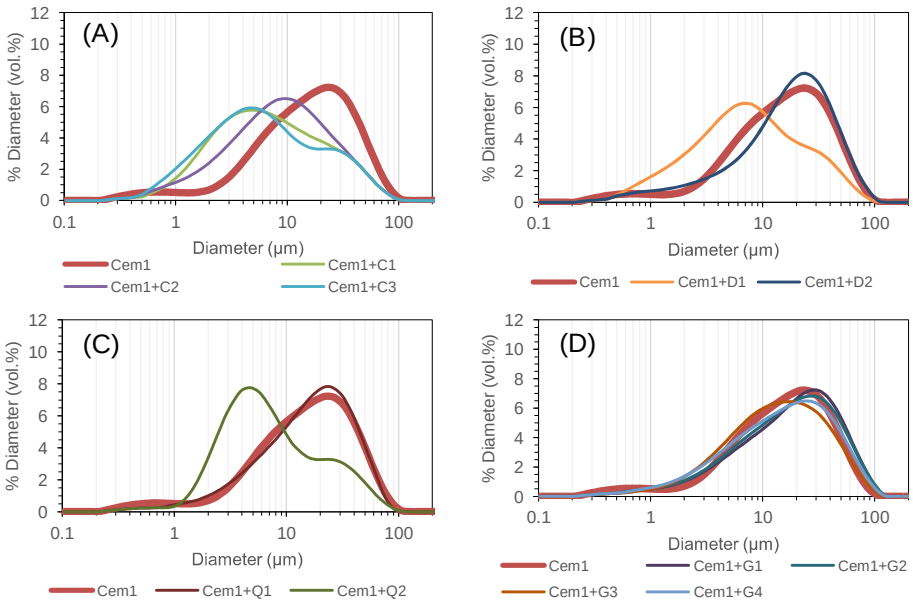

Fig. 6. Calculated particle size distribution of the blended systems (50% Cem1 + 50% SCM) compared to cement CEM 1: (A) cement and calcite, (B) cement and dolomite, (C) cement and quartz, (D) cement and granite.

Table 6
Suspensions characteristics: water content (vol.%), particles density (g/cm^3), specific surface area (SSA) (m^2/g), volumetric surface area (VSA) (m^2/cm^3), calculated minimum porosity (vol.%), interparticle separation distance (μm), and shape factor.

System		Water content (vol.%)	Density (g/cm^3)	SSA (m^2/g)	VSA (m^2/cm^3)	Porosity (vol.%)	IPS (μm)	ShF
Pure	Cem1	44.45	3.20	0.82	2.61	14.26	0.49	2.60
	Cem1	46.81	3.20	0.82	2.61	14.26	0.55	2.60
	D1	53.27	2.82	4.42	12.60	16.63	0.15	5.91
	D2	46.09	2.82	1.20	3.43	18.34	0.37	4.07
	C1	54.67	2.70	3.96	10.60	19.27	0.18	5.06
	C2	44.57	2.70	1.36	3.65	15.58	0.34	2.16
	C3	48.40	2.70	3.20	8.56	18.54	0.17	3.43
	Q1	51.46	2.65	1.00	2.64	16.62	0.65	3.96
	Q2	52.97	2.65	4.05	10.74	23.23	0.15	6.52
	G1	51.65	2.67	1.67	4.45	14.40	0.41	6.66
	G2	51.65	2.67	2.29	6.11	12.10	0.31	8.44
	G3	50.03	2.67	3.81	10.17	14.23	0.16	11.54
	G4	51.65	2.67	2.82	7.54	10.58	0.25	8.77
Blended	Cem1 + D1	42.98	3.01	2.62	7.89	13.94	0.15	4.25
	Cem1 + D1	37.62	3.01	2.62	7.89	13.94	0.11	4.25
	Cem1 + D2	42.98	3.01	1.01	3.04	16.43	0.37	3.33
	Cem1 + C1	42.18	2.92	2.39	6.96	14.50	0.16	3.83
	Cem1 + C2	42.18	2.92	1.09	3.18	14.10	0.36	2.38
	Cem1 + C2	36.85	2.92	1.09	3.18	14.10	0.26	2.38
	Cem1 + C3	42.18	2.92	2.01	5.85	14.00	0.19	3.01
	Cem1 + C3	36.85	2.92	2.01	5.85	14.00	0.14	3.01
	Cem1 + Q1	42.03	2.90	0.91	2.63	15.44	0.41	3.28
	Cem1 + Q2	42.03	2.90	2.43	7.06	18.72	0.14	4.56
	Cem1 + G1	42.13	2.91	1.24	3.62	13.66	0.32	4.63
	Cem1 + G2	42.13	2.91	1.55	4.52	12.89	0.26	5.52
	Cem1 + G3	42.13	2.91	2.31	6.73	14.10	0.17	7.07
	Cem1 + G4	42.13	2.91	1.82	5.30	12.36	0.22	5.68

by combination of unimodal suspensions viscosities cannot be considered as a true predictive model.

3.3. Sub-suspensions IPS distribution

An alternative model merging both the predictive concept of IPS with the particle interaction concept of Farris [42] is probably more capable of predicting the viscosity of multimodal suspensions. Such a combined approach was first introduced by Pileggi et al. [28] in alumina suspensions.

The central concept supporting this model assumes that a specific particle does not interact with other particles 10 times larger or 10 times smaller than its diameter. Conversely, the hard-solid interactions that affect the mobility of this particle in suspension, such as collisions, friction, and blockage, occur uniquely within ten times its diameter.

Consequently, the rheological behaviour of well-dispersed suspensions may be comprehended as an assembly of several sub-suspensions, each composed by the liquid phase and the particles around each specific particle size within the diameter ratio interval of ten times. Fig. 8 displays such a concept by plotting the effective particle size distributions around some exemplified diameters (125, 75, 45, 22.5, 11.25, 5.63, 2.37, 1.0, 0.5 and 0.25μm) of the cement tested in this work.

Each sub-suspension, defined for specific diameters, comprises the particles in its interference range size distribution immersed in the total liquid phase of the full suspension. Consequently, it is possible to calculate the specific particles and suspensions characteristics in each sub-suspension: the volumetric solid content (V_{si}), the volumetric surface area (VSA_i), the calculated pore fraction in the maximum packing condition according to Westman and Hugill model (P_{oi}) [39,41], and the suspension dimensionless relative density (dens.i), which is the suspension density relative to the liquid density. Fig. 9 exemplifies this

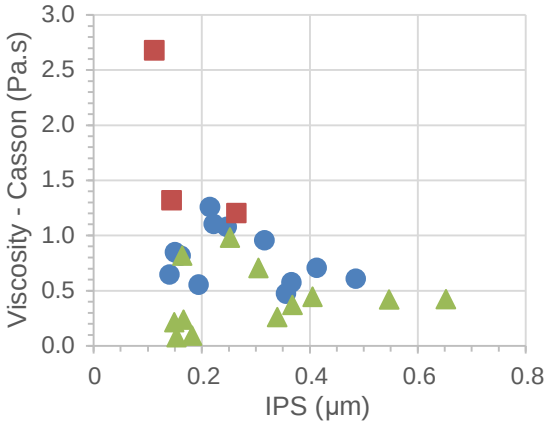

Fig. 7. Correlations of Casson's viscosity *versus* IPS. Green triangles are pure materials of w/s = 0.275–0.45; red squares are 50/50% cement-filler systems of w/s = 0.25; blue circles are 50/50% cement-filler systems of w/s = 0.20. (For interpretation of the references to colour in this figure legend, the reader is referred to the web version of this article.)

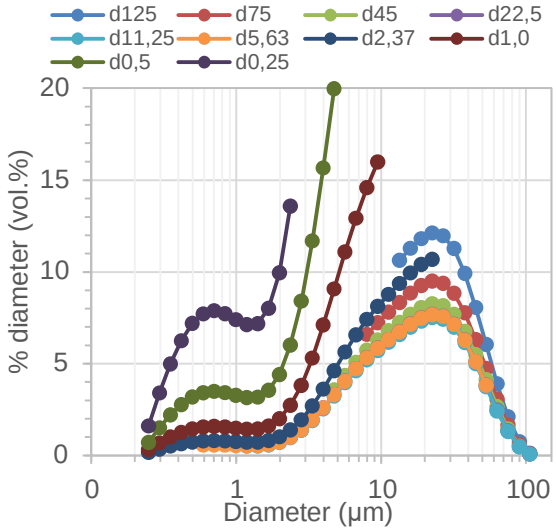

Fig. 8. Unitary particle distribution for some specific diameters (125, 75, 45, 22.5, 11.25, 5.63, 2.37, 1.0, 0.5, and 0.25 μm) of the tested cement considering the Farris 10× diameter ratio for particle interactions.

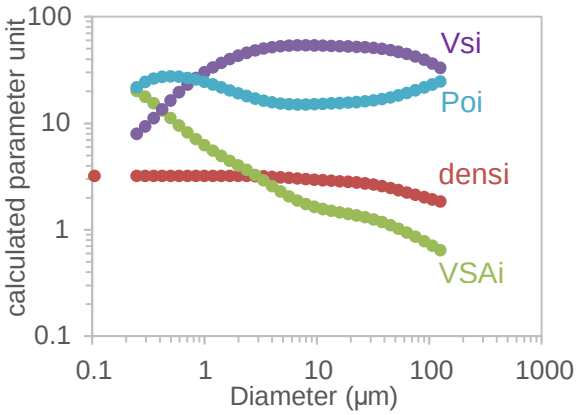

Fig. 9. Sub-suspensions characteristics for the tested cement: volumetric solid content Vsi; volumetric surface area VSAi (m^2/cm^3); calculated pore fraction in the maximum packing condition according (Poi); suspension relative density dens.i.

concept for the tested cement, but this approach is applicable for any suspension.

The convergence between the predictive IPS model with the particle interaction concept of Farris positively arises by calculating the IPS for each particle diameter sub-suspension. For that purpose, Eq. (1) is repeated for each sub-suspension using their specific characteristics, which are presented in Fig. 9. Indeed, Fig. 10 shows the calculated IPS distributions of the tested systems as a function of particle diameter.

In fact, each curve in Fig. 10 describes the IPS sub-suspension distributions for each cement, filler, and water combination, thus determining the available liquid space distribution around each particle's diameter. As observed, there is a great diversity in the IPS profiles and the IPS levels, so confirming the unique impact of the characteristics of each filler on the cement-based suspension. In contrast, the systems tested with distinct water content have similar profiles but with distinct IPS levels, as observed for the pairs Cem1 and Cem1 (0.275), Cem1 + C2 and Cem1 + C2 (0.2), Cem1 + C3 and Cem1 + C3 (0.2), and Cem1 + D1 and Cem1 + D1 (0.2).

It is also evident that the intermediate-sized particles' space for mobility is smaller than that of the particles with superior and inferior diameters. This feature is due to the absence of neighbouring particles 10 times larger or 10 times smaller than the diameter in these extremes. In view of this result, one might infer that the extreme particles in the size distribution have greater mobility than the intermediate ones.

However, this would be a mistaken inference because it would be assumed that similar spaces offer the same mobility potential for particles, independent of their differences in size. Furthermore, it would also be assumed that the energy dissipation phenomena that rule each particle movement have no influence on the suspension flow.

Therefore, more important than uniquely evaluating the IPS distributions is to relate the sub-suspensions distances with the characteristics that affect energy dissipation during the movement of particles. More precisely, surface forces and mass forces are the central forces governing energy dissipation. For that reason, aspects regarding friction, drag, collision, blockage, inertia, density, attractive/repulsive forces, among others, must be considered to understand particles movement capacity in the available space defined by IPS and consequently predict the viscosity of suspensions.

Pileggi et al. proposed this broad insight in the *Particles Interference Model* [28,32], which succeeded in correlating several physical aspects of particles and the immersing fluid to predict the viscosity of alumina ceramic suspensions.

3.3.1. The concept of interference (INT) and the viscosity

The basic idea that defines the interference model is the establishment of the spatial conditions for particle mobility by comparing the particle size and the mean free path among the particles defined by the IPS. According to this concept, larger particles require a larger IPS than smaller ones to have similar freedom conditions. This idea is easily comprehended in the schematic drawing in Figs. 11(A) and 12(A), where the same IPS is available for monosized particles with different diameters. In the first case, the particle size is larger than the IPS, thus hindering the movement of particles, independent of the IPS value (Fig. 11), and consequently increasing the energy dissipation and viscosity. In contrast, the particle size is smaller than the IPS in the second case (Fig. 12(A)), thus enabling particle mobility with a lower probability of energy dissipative interactions due to particles collisions, friction, liquid–solid drag disturbances, and instant localised capillary bridges, among others.

In addition to the spatial analysis, the interference model also evaluates the dissipative aspects regarding particles movement according to Stokes law [43] by calculating the potential decay distance travelled by a particle immersed in a liquid phase. The distance d_0 that a particle with diameter D_p and density ρ_s runs freely until stillness when projected horizontally at a speed v_0 in a liquid with viscosity η_f is described in Eq. (2).

$$d_0 = v_0 \cdot D_p^2 \cdot \frac{\rho_s}{18\eta_f} \quad (2)$$

where d_0 = distance travelled until the stillness (μm); v_0 = launching particle velocity (μm/s); D_p = particle diameter (μm); ρ_s = solid density (g/cm^3), and η_f = dynamic viscosity of the liquid (g/μm.s).

According to Eq. (2), it is possible to suppose that highly viscous liquids reduce the distance travelled by particles, thus diminishing the probability for hard solid contacts, independent of the particles size and IPS. In contrast, low viscous liquids facilitate particles movement and their inertial effects, thus enhancing the probability of collision among particles. In fact, the liquid viscosity impacts on the energy dissipated as heat during flow and particles movement.

Bearing in mind such concepts, the degree of freedom for the mobility of particles may be inferred by a proposed dimensionless parameter named dynamic interference (INT_d), which was defined as the ratio between the maximum distance (d_0) that a particle launched at a certain velocity v_0 may travel until the particle is stopped and the mean distance to other particles, as calculated using the IPS model. Eq. (3) describes the dynamic interference (INT_d) of monomodal suspensions as follows [32]:

$$INT_d = v_0 \cdot \frac{D_p^2}{IPS} \cdot \frac{\rho_s}{18\eta_f} \quad (3)$$

where v_0 = launching particle velocity (μm/s); D_p = particle diameter (μm); IPS = particle separation distance (μm); ρ_s = solid density (g/cm^3), and η_f = dynamic viscosity of the liquid (g/μm.s).

The dimensionless dynamic interference includes both extrinsic and intrinsic aspects of the suspension. However, the intrinsic characteristics of the suspensions can be identified through dividing INT_d by v_0, thus defining the natural interference (INT_n) of the system by Eq. (4) [32].

$$INT_n = \frac{D_p^2}{IPS} \cdot \frac{\rho_s}{18\eta_f} \quad (4)$$

This equation determines the time required to overcome a unit of distance (time/distance). In effect, the involved parameters consider the mobility potential of the particles regarding their spatial freedom degree and the inertial effects. Therefore, INT_d permits predictive comparisons among different suspensions, independent of their shearing conditions.

However, the adequacy of this model for viscosity description of monomodal suspensions is only possible by introducing an experimental

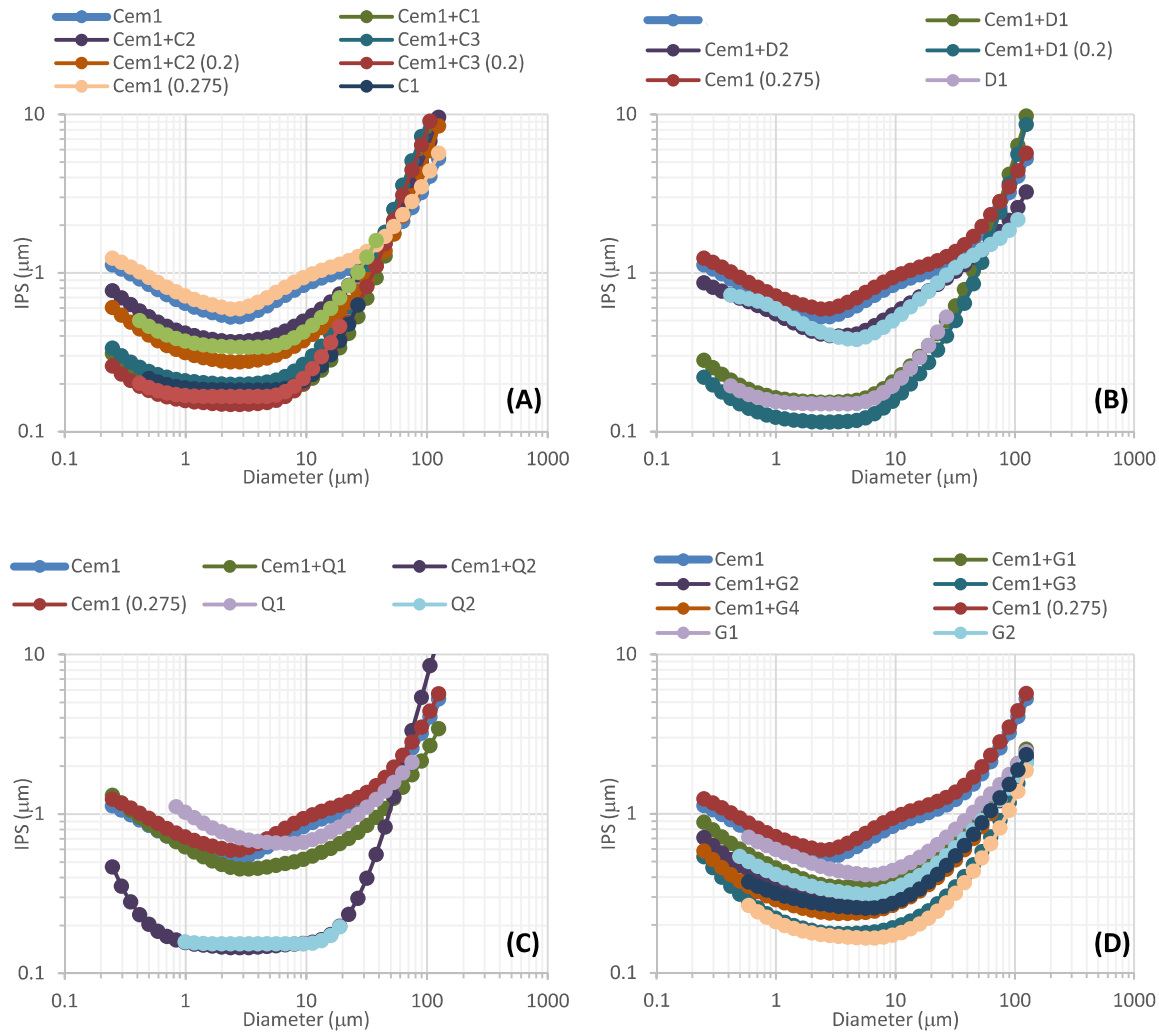

Fig. 10. Calculated IPS for each diameter sub-suspension considering the interference interval ratio of 10×: (A) cement and calcite, (B) cement and dolomite, (C) cement and quartz, (D) cement and granite.

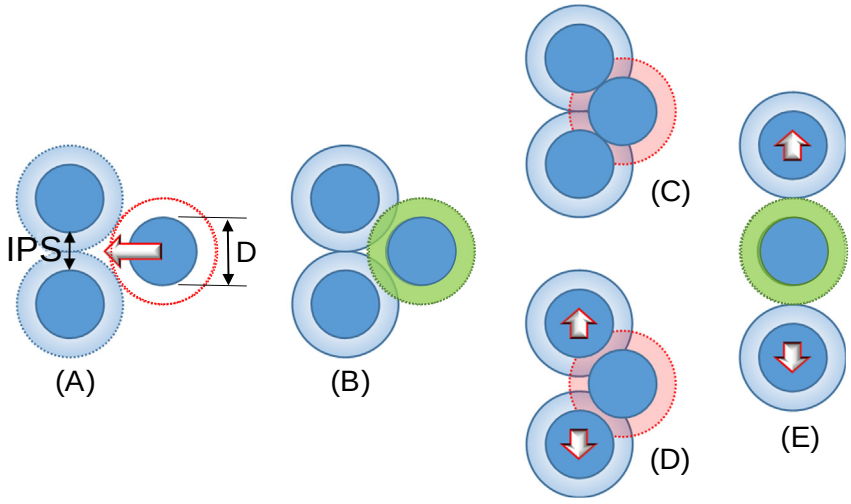

Fig. 11. Schematic representation of the suspensions of particles of diameter larger than IPS: (A) initial condition where all particles are equally distant by the IPS, with the arrow indicating the movement direction of the mobile particle; (B) mobile particle stopped before collision (green IPS layer indicates the absence of collision) with the others; (C) mobile particle hard solid collision (red IPS layer indicates movement blockage) with the others; (D) overlapping IPS layers decelerates the mobile particle and induces movement to the others; (E) mobile particle moves freely among the others due to their movement of separation. (For interpretation of the references to color in this figure legend, the reader is referred to the web version of this article.)

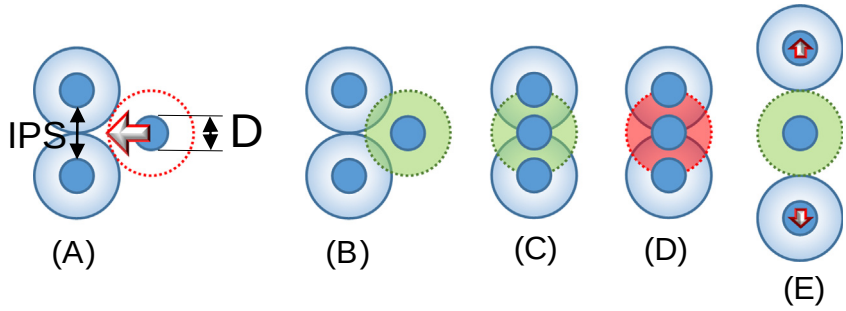

Fig. 12. Schematic representation of suspensions of particles with diameter smaller than the IPS: (A) initial condition where all of the particles are equally distant by the IPS, with the arrow indicating the movement direction of the mobile particle; (B) mobile particle stopped before collision (green IPS layer indicates absence of collision) with the others; (C) mobile particle moves among the others without being affected by the IPS layers overlapping; (D) mobile particle moves among the others while being affected by the IPS layers overlapping; (E) mobile particle moves freely among the others due to their movement of separation. (For interpretation of the references to colour in this figure legend, the reader is referred to the web version of this article.)

parameter (H) to consider other energy dissipation sources and the experimental conditions to measure viscosity. The final interference model is then proposed in Eq. (5) [32].

$$INT = H x \frac{D_p^2}{IPS} \cdot \frac{\rho_s}{18\eta_f} \quad (5)$$

The suspension constant H was proven to be related to the number of particles per unit of volume, the surface area, the solid density, and the liquid viscosity. The physical meaning of the suspension constant involves the suspension capacity of energy dissipation in terms of heat during the experimental measure of viscosity, but it still requires further investigation.

The expansion of the interference model from monomodal to multimodal systems is possible by adopting the sub-suspensions concept for particle interaction. In fact, the bulk interference in a multimodal system accounts for each single-diameter interference value, assuming that the IPS is calculated inside its sub-suspension, while considering its volumetric contribution in the suspension. This statement addresses the mixing law for bulk properties so that the interference for multimodal suspensions (INT_{ni}) was proposed to be the sum of each diameter natural interference multiplied by its volumetric contribution in the suspension, as seen in Eq. (6).

$$INT_{ni} = \sum_{i=1}^{m} x_i \cdot INT_i \quad (6)$$

where x_i = volumetric content of particle with diameter D_i, INT_i = Natural Interference calculated for particle D_i assuming the IPS calculated inside its sub-suspension; m = number of size diameters.

However, the concept of sub-suspensions alters the comprehension of the natural interference in Eq. (4). In effect, each particle flows inside its sub-suspension, so that the sub-suspension density affects its inertia in the system. For that reason, the particle solid density (ρ_s) must be related to the sub-suspension density by adopting its dimensionless relative density (ρ_r). Moreover, to retain the natural interference time/distance concept, the inertial effect from the liquid phase (water) also must be discounted by assuming the kinematic viscosity (η_k), which is defined as the ratio between the dynamic liquid viscosity (η_f) and its density (ρ_{liq}) [32]. Therefore, the natural interference (INT_i) calculated for a particle with a certain diameter D_{pi} is described in Eq. (7)

$$INT_i = \frac{D_{pi}^2}{IPS_i} \cdot \frac{\rho_r}{18\eta_k} \quad (7)$$

where D_{pi} = particle with diameter D_i, IPS_i = particle separation distance in the sub-suspension defined around the diameter D_i, ρ_r = dimensionless relative density, η_k = kinematic viscosity of the liquid.

The interferences of the pure and blended systems tested in the present work were calculated using the sub-suspensions characteristics previously presented. First, Fig. 13 displays the linear relation between the natural interference (INT_{ni}) and the Casson viscosities. In fact, viscosity increased with INT_{ni}, but three distinct major trend curves could be fitted according to the water/solid ratio of the suspensions.

Such divergences were predictable because natural interference INT_{ni} does not consider the experimental H parameter, which is supposedly associated with the energy dissipation phenomena in suspensions that are activated as a result of the experimental setup adopted for measuring viscosity. To improve viscosity prediction, Fig. 14 demonstrates the very good linear correlation between interference (INT_p) and Casson viscosity when INT_{ni} is adjusted by the H parameter calculated to minimise deviation from the linear function.

Therefore, the interference of multimodal suspensions is finally described by Eq. (8):

$$INT_p = H \cdot \sum_{i=1}^{m} x_i \cdot INT_{ni} \quad (8)$$

where H = experimental dissipation parameter; x_i = volumetric content of particles with diameter D_i; INT_{ni} = Natural interference

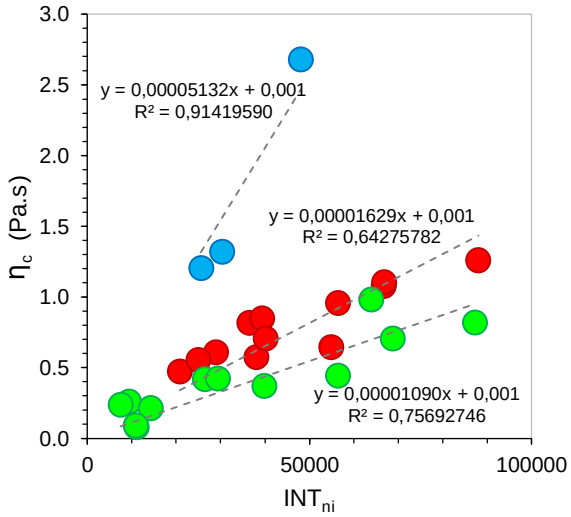

Fig. 13. Casson's viscosity *versus* Natural interference (INT_{ni}). Green circles are pure materials of w/s = 0.275–0.45; red circles are 50/50% cement-filler systems of w/s = 0.25; blue circles are 50/50% cement-filler systems of w/s = 0.20. (For interpretation of the references to colour in this figure legend, the reader is referred to the web version of this article.)

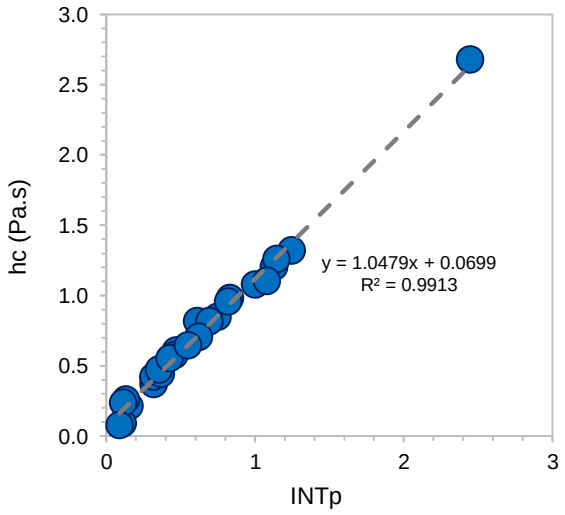

Fig. 14. Linear relation between Casson's viscosity *and* Interference (INT_p).

calculated for particle D_i assuming the IPS calculated inside its sub-suspension; m = number of size diameters.

To confirm the physical significance of this linear relationship, it is necessary to determine the H adjustment parameter regarding the characteristics of the suspensions. Indeed, the calculated values of the H adjustment parameter displayed a good relationship with the volumetric solid content in the suspensions, as shown in Fig. 15.

The rate of H increase was small for the lower solid content but increased exponentially at high concentrations. This result endorses this experimental parameter as the one that accounts for the energy dissipation in terms of heat in the interference model, as originally described. This hypothesis assumes the increase of hard solid contacts, such as collisions and surface friction, by increasing the amount of solid particles in sheared suspension and the decrease of the heat dissipation capacity caused by the lower water content.

As observed, the shape of the H × volume solid content curve is similar to the concentration dependence of viscosity in the well established models presented in Table 5 [23–27]. Assuming this fact, it can infer that the interference model estimate viscosity from fundamental measured characteristics of the particles and liquid, without the need to assume values for the intrinsic viscosity and the critical solid concentration. Moreover, it is possible to use the interference theory to calculate the

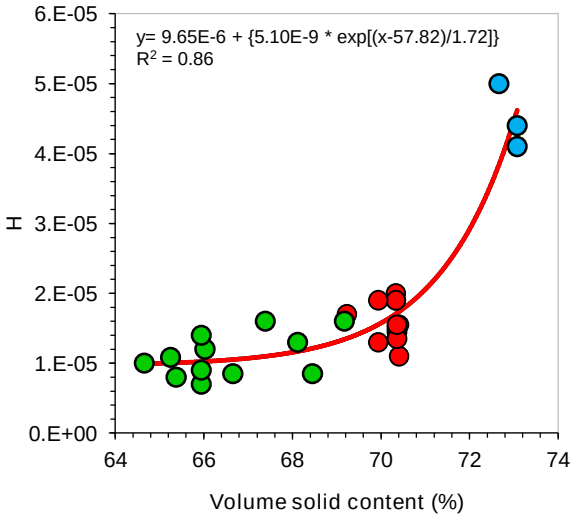

Fig. 15. Relationship of the experimental energy dissipative parameter with the volume solid content.

critical solid content or the intrinsic viscosity that are usually supposed in viscosity predictive models like those from Table 5. This possibility enlarges the field for comprehension regarding the physical significance of both parameters, but the true significance of the H parameter continue to demand investigation.

4. Concluding remarks

The increase in the efficiency of binder use is required for the future low CO_2 society. Binder optimization by replacing part of the clinker with inert supplementary cementitious materials (SCM) has enormous potential to supply the cement-based materials that society needs while reducing the environmental impacts. However, the wide range of different fillers available worldwide can make this replacement very difficult because they have very different characteristics (size distribution, shape, density) that affect the rheological behaviour when combined with clinker.

Although not a complete theoretical model, the interference concept demonstrated good performance to describe the Casson viscosity of 27 suspensions tested in this work, including pure and blended pastes using 11 different fillers. Considering that the interference values are calculated based on the fundamental characteristics of the suspensions, it is possible to infer its adequacy as a predictive model, once the experimental relation between the dissipative parameter H and the solid volumetric content was established.

In that sense, this model estimates the viscosity of suspensions based on the different aspects of the liquid phase (density and viscosity) and the particles, including density, viscosity, size distribution, surface area and its determining factors, such as shape, roughness, and porosity. For that reason, the interference model is an important tool capable to enhance the use of innovative supplementary cementitious materials in cementitious suspensions.

Even if the results are not definitive, the results presented herein are encouraging. If used properly, the proposed interference model is capable to collaborate with CO_2 mitigation in the production of cement-based materials. Based on its accuracy of the viscosity prediction, this model enables a systematic method for selection of SCMs in clinker replacement because it allows the estimation of the water demand for achieving the particles mobility necessary to a demanded viscosity. This conclusion is certainly important because the final properties of cement-based materials in hardened state depend on the water content used during its processing in the fresh state.

Acknowledgements

Dr. Bruno Damineli's work was supported by FAPESP – Fundação de Amparo à Pesquisa do Estado de São Paulo (grant 2013/03688-3). The information and views presented in this study are those of the authors and do not necessarily reflect the opinion of FAPESP. The authors also thank Dr. Fabio A. Cardoso for revising the paper.

References

[1] World Business Council for Sustainable Development (WBCSD), The cement sustainability initiative (CSI), CSI Report, 2007 (8p.).
[2] N. Müller, J. Harnish, A blueprint for a climate friendly cement industry, WWF-Lafarge Partnership Report, WWF Lafarge Conservation Partnership, Gland, 2008 (94p.).
[3] E. Gartner, Industrially interesting approaches to "low CO2" cements, Cem. Concr. Res. 34 (2004) 1489–1498.
[4] B.L. Damineli, V.M. John, Developing low CO2 concretes: is clinker replacement sufficient? The need of cement use efficiency improvement, Key Eng. Mater. 517 (2012) 342–351.
[5] S. Anderson, R. Newell, Prospects for carbon capture and storage technologies, Annu. Rev. Environ. Resour. 29 (2004) 109–142.
[6] V. Hoenig, H. Hoppe, B. Emberger, Carbon capture technology – options and potentials for the cement industry, PCA R&D Serial no. 3022 (Technical Report), European Cement Research Academy, Germany, 2007 (98p.).
[7] World Business Council For Sustainable Development (WBCSD)/International Energy Agency (IEA), Cement Technology Roadmap 2009 – Carbon Emissions Reductions up to 2050, 2009 (36p.).

[8] B.L. Damineli, F. Kemeid, P.A. Silva, V.M. John, Measuring the eco-efficiency of cement use, Cem. Concr. Compos. 32 (2010) 555–562.
[9] G. Habert, N. Roussel, Study of two concrete mix-design strategies to reach carbon mitigation objectives, Cem. Concr. Compos. 31 (2009) 397–402.
[10] G. Habert, E. Denarié, A. Sajna, P. Rossi, Lowering the global warming impact of bridge rehabilitations by using ultra high performance fibre reinforced concretes, Cem. Concr. Compos. 38 (2013) 1–11.
[11] Cementitious Slag Makers Association (CSMA), Fact Sheet 18 – Embodied CO2e of UK cement, additions and cementitious material, Available: http://www.ukcsma.co.uk/files/Factsheet_18_CO2e_of_Cementitious_Materials_2012.pdf
[12] P.D. Tennis, M.D.A. Thomas, W.J. Weiss, State-of-the-Art Report on Use of Limestone in Cements at Levels of up to 15%, Portland Cement Association, Skokie, Illinois, USA, 2011 (Available: bhttp://www.cptechcenter.org/projects/ncc/SN3148_Use%20of%20Limestone%20in%20Cements.pdfN).
[13] B. Lothenbach, G.L. Saout, E. Gallucci, K. Scrivener, Influence of limestone on the hydration of Portland cements, Cem. Concr. Res. 38 (2008) 848–860.
[14] B. Lothenbach, K. Scrivener, R.D. Hooton, Supplementary cementitious materials, Cem. Concr. Res. 41 (2011) 217–229.
[15] BS EN 197-1:2011, Cement Composition, Specifications and Conformity Criteria for Common Cements, September 2011.
[16] K.L. Scrivener, R.J. Kirkpatrick, Innovation in use and research on cementitious material, Cem. Concr. Res. 38 (2008) 128–136.
[17] Y. Knop, A. Peled, Packing density modeling of blended cement with limestone having different particle sizes, Constr. Build. Mater. 102 (2016) 44–50.
[18] R. Buscall, I.J. McGowan, P.D.A. Mills, R.F. Stewart, D. Sutton, L.R. White, G.E. Yates, The rheology of strongly flocculated suspensions, J. Non-Newtonian Fluid Mech. 24 (1987) 183–202.
[19] P.C. Kapur, P.J. Scales, D.V. Boger, T.W. Healy, Yield stress of suspensions loaded with size distributed particles, AICHE J. 43 (1997) 1171–1179.
[20] P.J. Scales, S.B. Johnson, T.W. Healy, P.C. Kapur, Shear yield stress of partially flocculated colloidal suspensions, AICHE J. 44 (1998) 538–544.
[21] Z. Zhou, M.J. Solomon, P.J. Scales, D.V. Boger, The yield stress of concentrated flocculated suspensions of size distributed particles, J. Rheol. 43 (1999) 651–671.
[22] R.J. Flatt, P. Bowen, Yodel: a yield stress model for suspensions, J. Am. Ceram. Soc. 89 (2006) 1244–1256.
[23] I.M. Krieger, T.J. Dougherty, A mechanism for non-Newtonian flow in suspensions of rigid spheres, Trans. Soc. Rheol. III (1959) 137–152.
[24] M. Mooney, The viscosity of a concentrated suspension of spherical particles, J. Colloid Interface Sci. 6 (2) (1951) 162–170.
[25] H. Eilers, Die Viskosität von Emulsionen hochviskoser Stoffe als Funktion der Konzentration, Kolloid Z. 97 (3) (1941) 313–321.
[26] D. Quemada, Rheology of concentrated disperse systems and minimum energy dissipation principle – I. Viscosity concentration relationship, Rheol. Acta 16 (1977) 82–94.
[27] J.V. Robinson, The viscosity of suspensions of spheres, J. Phys. Chem. 53 (7) (1949) 1042–1056.
[28] R.G. Pileggi, A.R. Studart, V.C. Pandolfelli, Um modelo para previsão da viscosidade mínima de suspensões cerâmicas, Cerâmica, Brasil 46 (299) (2000) 160–165 (in portuguese).
[29] M. Hunger, H.J.H. Brouers, Flow analysis of water-powder mixtures: application to specific surface area and shape factor, Cem. Concr. Compos. 31 (2009) 39–59.
[30] S.T. Erdogan, X. Nie, P.E. Stutzman, E.J. Garboczi, Micrometer-scale 3-D shape characterization of eight cements: particle shape and cement chemistry, and the effect of particle shape on laser diffraction particle size measurement, Cem. Concr. Res. 40 (2010) 731–739.
[31] S.A.A.M. Fennis, Measuring water demand or packing density of micro powders – comparison of methods, Research paper, Delft University of Technology, Civil Engineering and Geosciences, Institutional Repository, 2008 (Available: bhttp://repository.tudelft.nl/view/ir/uuid:9f1a716d-d669-4ce5-9fae-1afefac2c168N, 21p).
[32] I.R. Oliveira, A.R. Studart, R.G. Pileggi, V.C. Pandolfelli, Dispersão e empacotamento de partículas – princípios e aplicações em processamento cerâmico, Fazendo Arte Editorial, São Paulo, 2000 224 p (in portuguese).
[33] K. Yoshioka, E.I. Tazawa, K. Kawai, T. Enohata, Adsorption characteristics of superplasticizers on cement component minerals, Cem. Concr. Res. 32 (2002) 1507–1513.
[34] C. Jolicoeur, M.A. Simard, Chemical admixture-cement interactions: phenomenology and physico-chemical concepts, Cem. Concr. Compos. 20 (1998) 87–101.
[35] N. Mikanovic, C. Jolicoeur, Influence of superplasticizers on the rheology and stability of limestone and cement pastes, Cem. Concr. Res. 38 (2008) 907–919.
[36] N. Gence, N. Ozbay, pH dependence of eletrokinetic behavior of dolomite and magnesite in aqueous electrolyte solutions, Appl. Surf. Sci. 252 (2006) 8057–8061.
[37] M. Nehdi, M.A. Rahman, Estimating rheological properties of cement pastes using various rheological models for different test geometry, gap and surface friction, Cem. Concr. Res. 34 (2004) 1993–2007.
[38] A. Dörr, A. Sadiki, A. Mehdizadeh, A discrete model for the apparent viscosity of polydisperse suspensions including maximum packing fraction, J. Rheol. 57 (3) (2013) 743–765.
[39] J.E. Funk, D.R. Dinger, Predictive Process Control of Crowded Particulate Suspensions Applied to Ceramic Manufacturing, Kluwer Academic Publishers, Boston/Dordrecht/London, 1994 (765p.).
[40] F. Ortega, R.G. Pileggi, A.R. Studart, V.C. Pandolfelli, IPS as a viscosity-predictive parameter, Am. Ceram. Soc. Bull. 81 (1) (2002) 44–52.
[41] A.E.R. Westman, H.R. Hugill, The packing of particles, J. Am. Ceram. Soc. 13 (1930) 767–779.
[42] R.J. Farris, Prediction of the viscosity of multimodal suspensions from unimodal viscosity data, Trans. Soc. Rheol. 12 (2) (1968) 281–301.
[43] M. Rhodes, Introduction to Particle Technology, second ed. John Wiley & Sons Ltd., 2008 (472p.).